AGU PUBLICATIONS

Geophysical Research Letters

RESEARCH LETTER
10.1002/2016GL068204

Key Points:
- Directions of tilt in the pack ice shows narrow long-period swell beams that are not compatible with a strong scattering
- Swell attenuation rates inferred from model-data comparisons are 12 times larger than under-ice viscous friction
- Dissipation rates are compatible with secondary creep effects

Correspondence to:
F. Ardhuin,
ardhuin@ifremer.fr

Citation:
Ardhuin, F., P. Sutherland, M. Doble, and P. Wadhams (2016), Ocean waves across the Arctic: Attenuation due to dissipation dominates over scattering for periods longer than 19 s, *Geophys. Res. Lett.*, *43*, 5775–5783, doi:10.1002/2016GL068204.

Received 11 FEB 2016
Accepted 23 MAR 2016
Accepted article online 28 MAR 2016
Published online 6 JUN 2016

Ocean waves across the Arctic: Attenuation due to dissipation dominates over scattering for periods longer than 19 s

Fabrice Ardhuin[1], Peter Sutherland[1], Martin Doble[2], and Peter Wadhams[3]

[1]University Brest, CNRS, IRD, Ifremer, Laboratoire d'Océanographie Physique et Spatiale (LOPS), IUEM, Brest, France, [2]Polar Scientific Ltd, Appin, UK, [3]Department of Applied Maths and Theoretical Physics, University of Cambridge, Cambridge, UK

Abstract The poorly understood attenuation of surface waves in sea ice is generally attributed to the combination of scattering and dissipation. Scattering and dissipation have very different effects on the directional and temporal distribution of wave energy, making it possible to better understand their relative importance by analysis of swell directional spreading and arrival times. Here we compare results of a spectral wave model—using adjustable scattering and dissipation attenuation formulations—with wave measurements far inside the ice pack. In this case, scattering plays a negligible role in the attenuation of long swells. Specifically, scattering-dominated attenuation would produce directional wave spectra much broader than the ones recorded, and swell events arriving later and lasting much longer than observed. Details of the dissipation process remain uncertain. Average dissipation rates are consistent with creep effects but are 12 times those expected for a laminar boundary layer under a smooth solid ice plate.

1. Introduction

Arctic sea ice is undergoing rapid changes in extent and thickness [e.g., *Maslanik et al.*, 2007; *Renner et al.*, 2014] that are poorly reproduced by numerical models [e.g., *Stroeve et al.*, 2014], leading to large errors in air-sea fluxes in both long-range climate forecasts and short-term operational weather forecasts. Besides the impact of air and water temperatures on the melting of sea ice [e.g., *Lique et al.*, 2014], and the albedo feedback [e.g., *Perovich et al.*, 2007], ocean waves can also enhance ice retreat as bigger waves may lead to more ice break up which generally results in bigger waves due to the increased fetch [*Thomson and Rogers*, 2014]. It is then suspected that, with reduced ice cover, the consequent energetic waves are more effective in breaking up the ice [e.g., *Asplin et al.*, 2012] and mixing the upper ocean, thereby favoring melting and a further reduced ice extent.

The region where ice is broken by waves is the marginal ice zone (MIZ), and its extent is directly controlled by the attenuation rate of waves propagating into the ice. The causes and magnitude of this attenuation have been strongly debated over the last 40 years, and various feedbacks of ice properties on wave attenuation have been proposed [e.g., *Squire and Moore*, 1980]. Here we focus on particularly long-period waves and measurements far inside of the ice pack. That particular regime may be relevant to the MIZ evolution as it probably involves some of the wave-ice interaction processes that define the wave attenuation before the ice is broken. However, our data set is limited to measurements far in the ice, which do not allow a separation of MIZ processes from ice pack processes, and effectively only constrains the latter.

Broken ice floes [e.g., *Meylan et al.*, 1997; *Montiel et al.*, 2016] or variations in ice thickness [*Squire et al.*, 2009; *Bennetts and Squire*, 2012] may scatter wave energy in all directions thereby enhancing the wave attenuation. Alternatively, the breaking of ice into small floes reduces the deformations of the ice layer, resulting in less creep-induced dissipation of wave energy, possibly explaining the weak attenuation of waves in broken ice reported by *Collins et al.* [2015], compared to similar wave conditions in unbroken ice. The reader is referred to the reviews by *Squire et al.* [1995] and *Mosig et al.* [2015] for a presentation of other possible dissipation mechanisms and parameterizations.

Clearly, a knowledge of wave attenuation mechanisms in sea ice is necessary to allow a quantitative prediction of the MIZ extent [e.g., *Dumont et al.*, 2013; *Williams et al.*, 2013a, 2013b]. From observations of heave alone [e.g., *Wadhams*, 1975; *Squire and Moore*, 1980; *Wadhams et al.*, 1988], the attenuation of wave energy can be attributed to many different processes that can then be parameterized into numerical models [*Doble and Bidlot*, 2013]. Including observations of directional wave properties in the ice allows discrimination between

scattering, which tends to broaden the directional spectrum and can dominate for short-period waves in the MIZ [e.g., *Squire et al.*, 1995] and dissipation — whatever the physical process at play — which tends to produce narrow spectra as the obliquely traveling waves are more attenuated because of their longer propagation path [*Wadhams*, 1978; *Squire et al.*, 1995]. Thus, the directional spread of the wave spectrum is a key diagnostic parameter that reveals the relative importance of scattering and dissipation due to wave-ice interactions, as it does in coastal waters due to wave-bottom interactions [*Ardhuin et al.*, 2003].

In this work, we analyze wave data collected in the vicinity of the schooner *Tara* during its 2007 trans-Arctic drift experiment. The data set is compared to a numerical wave model that simulates attenuation of waves in ice due to scattering and/or dissipation.

2. Waves Measurements on the Ice

Wadhams and Doble [2009] measured the slopes of the ice surface in two orthogonal directions, x and y, using tiltmeters. The instruments were not equipped with heading sensors, meaning that the absolute orientation of these directions could not be determined. However, in this work we focus on the directional spreading, which has no dependence on absolute orientation.

Assuming the wave-induced surface elevation is linear, it can be written as

$$\zeta(x,y,t) = \sum_{i,j} a_{i,j} \cos\left(k_i x \cos\theta_j + k_i y \sin\theta_j - 2\pi f_i t + \phi_{i,j}\right) \tag{1}$$

$$= \sum_{i} Z_i \cos\left(2\pi f_i t + \psi_i\right) \tag{2}$$

which is composed of monochromatic and long-crested waves each with amplitude $a_{i,j}$, wave number k_i, direction θ_j, frequency f_i and random phase $\phi_{i,j}$ in the two-dimensional spectrum and ψ_i for the frequency spectrum. Taking the horizontal gradients of equation (1), the surface slopes are similar sums of sines, multiplied by $-k_i \cos\theta_i$ for slopes in the x direction and by $-k_i \sin\theta_i$ for slopes in the y direction.

The spectra C_{xx} and C_{yy} and cospectrum C_{xy} of the slopes provide information on the slope variance and can be related to the elevation spectrum, $E(f)$, using the dispersion relation. In this case, the linear deep water dispersion relation for open water, $\sigma^2 = gk$, was used. Because we focus on wave period longer than 19 s and ice thickness under 4 m, ignoring ice effects in the dispersion relation is considered acceptable [e.g. *Wadhams and Doble*, 2009]. From equation (2), the heave spectrum is obtained by taking the average of records of the discrete Fourier transform $E(f) = \langle \zeta(f_i)^2 \rangle$, which is a sum of the variance over all directions j. The slope spectra $C_{xx}(f)$ and $C_{yy}(f)$ are simply the sums over directions of the directional heave spectrum $F(f,\theta)$ multiplied by $k^2 cos^2\theta$ and $k^2 sin^2\theta$, respectively. Likewise, the cross spectrum C_{xy} is the sum of $E(f)$ multiplied by $k^2 \cos\theta \sin\theta$.

As a result, without making any assumptions regarding the shape of $F(f,\theta)$, the directional spreading, $\sigma_2(f)$, can be estimated. This spreading is defined here from the second moments of the directional distribution, $F(f,\theta)$, with

$$a_2 = (C_{xx} - C_{yy})/(C_{xx} + C_{yy}) = \int \cos(2\theta) F(f,\theta) \mathrm{d}\theta, \tag{3}$$

$$b_2 = (2C_{xy})/(C_{xx} + C_{yy}) = \int \sin(2\theta) F(f,\theta) \mathrm{d}\theta, \tag{4}$$

$$m_2(f) = \sqrt{a_2^2(f) + b_2^2(f)}, \tag{5}$$

$$\sigma_2(f) = \sqrt{(1 - m_2)/2}. \tag{6}$$

Although this definition is slightly different from the one in *Kuik et al.* [1988], it is well adapted to data in which the first moment of the spectrum is not available because we do not have a direct measurement of the heave. In the limit of a narrow Gaussian spectrum, σ_2 is the half width (standard deviation) of that spectrum.

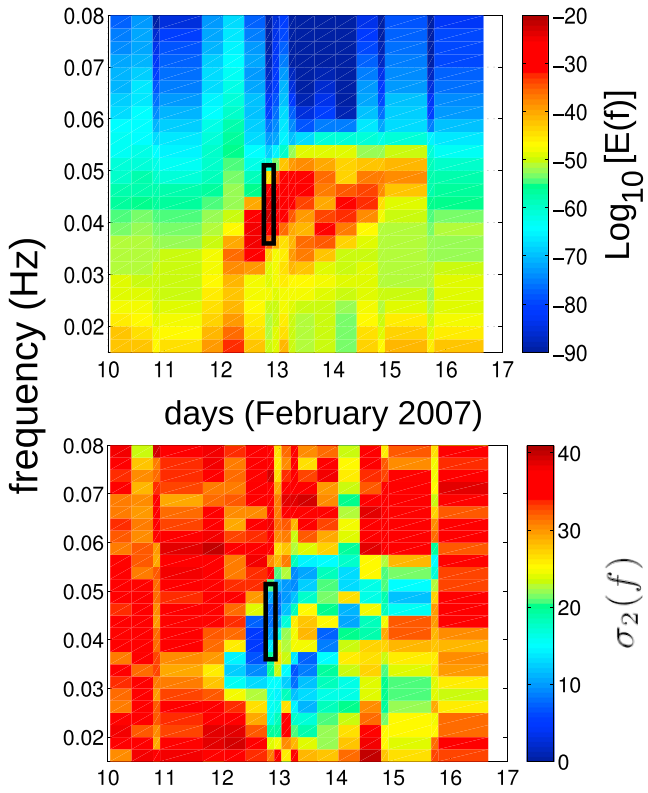

Figure 1. (top) Spectrogram of surface elevation, (bottom) width of the directional wave spectrum estimated from second moments (equation (6)). The black rectangle highlights the time and frequency range of the spectral peak on 12 February at 18:00 UTC, showing that the directional spreading is around 10° or less when the energy is maximum. This spectral range is used in Figures 2a, 2b, and 3.

The spectra and cospectra were computed using the *Welch* [1967] method with half-overlapping records of 400 s and a Hanning window. We also corrected for a processing error in *Wadhams and Doble* [2009], where the sampling frequency $f_s = 2.18$ Hz was erroneously reduced by a factor 1.5. Spectra were averaged over each data burst, which have a variable length from 0.5 to 3 h. Records were excluded from the average if the maximum tilt change over a sampling interval exceeded half of the standard deviation of that record, or if the standard deviation of the record was 3 times larger than that of the data burst. This filtering is useful for bursts later in the year, from April to June, with many spikes caused by floe-floe collisions in the more open and mobile ice cover. For our period of interest, from 12 to 15 February, less than 5% of the record have been removed for each burst, and a visual inspection of the data reveals apparent wave packets, typical of narrow-banded spectra.

Figure 1 shows the heave spectrum and directional spreading σ_2 estimated from one of the two-axes tiltmeters. The week starting on 10 February is marked by two events in close succession. The frequency f_p at which the heave spectrum $E(f)$ is maximum, has the usual linear increase with time, $\mathrm{d}f_p/\mathrm{d}t = g/(4\pi X)$, that is characteristic of the dispersive arrival of swells from remote sources at a distance X [e.g., *Munk et al.*, 1963; *Delpey et al.*, 2010]. The sources of the swells on 9 and 10 February were determined to be approximately 5000 km from the sensors, allowing the storms that generated the swells to be isolated. Both events were major storms that peaked west of Ireland, with maximum significant wave heights H_s of 19.5 m at 48°N 25°W on 9 February at 15:00 UTC, and 18.5 m at 48°N 31°W on 10 February at 12:00 UTC. These estimates are based on a well-calibrated numerical wave model [*Rascle and Ardhuin*, 2013], forced by winds from the Climate Forecasting System Reanalysis (CFSR) [*Saha et al.*, 2010] and confirmed by satellite altimeter data [*Queffeulou and Croizé-Fillon*, 2010]. That model has a H_s bias under 5% for H_s up to 18 m, and a scatter index under 10% for H_s values above 10 m.

These are the two biggest wave events on Earth for that month, associated with two storms moving at speeds close to the dominant wave group speed. These storms are very similar to the Quirin storm of February 2011,

which has the largest measured sea state in the satellite altimetric record [*Hanafin et al.*, 2012] and which was well represented by the same numerical model configuration. All three storms generated swells with peak periods exceeding 25 s outside of the ice. The swells studied here were able to reach the Arctic through a relatively narrow window between Iceland and Svalbard. The short duration in the storms intensity together with this narrow window explains the succession of two well-defined events.

The directional spreading in Figure 1b shows that when the energy level is maximum, the measured spectrum is very narrow. Since the spreading is defined using the second moments of the directional distribution, it is possible that the spectrum is the combination of two narrow beams in exactly opposite direction, each with a half width under 10°. Since we know of no natural geophysical process that could backscatter these waves uniquely in the exact opposite direction, we interpret this data as a single narrow beam of energy, indicating that the attenuation of these swells is mostly due to dissipative processes. This interpretation is consistent with the numerical wave model results discussed in the next section.

3. Modeling of Wave Dissipation and Scattering

In order to evaluate the possible impact of scattering and dissipation, we have nested a curvilinear grid configuration of the WAVEWATCH III model into the global wave hindcast of *Rascle and Ardhuin* [2013]. The polar grid is the same as that used for the daily 12.5 km resolution maps of sea ice concentration derived from the Special Sensor Microwave Imager (SSM/I) [*Ezraty et al.*, 2007]. The SSM/I ice concentration c and CFSR wind fields were used to force the model. The model is also forced at its open boundary at 66 N using directional spectra from the global wave model of *Rascle and Ardhuin* [2013]. The Arctic grid includes a 50 km artificial island at the North Pole, in order to avoid errors in the refraction scheme, because we are using true north as a reference direction. The spectral grid uses 24 directions and 33 frequencies from 0.0338 to 0.7 Hz. The addition of lower frequency components with sources of infragravity waves [*Ardhuin et al.*, 2014] or a finer directional distribution did not significantly change the dominant swell properties.

Waves are propagated through the ice using two very simple parameterizations of dissipation and scattering. A recent review of more complex dissipation models is presented in *Mosig et al.* [2015]. Here we represent dissipation by the under-ice laminar friction theory of *Liu and Mollo-Christensen* [1988] in which the viscosity is set to the molecular viscosity at the freezing temperature of sea water, $\nu \simeq 1.83 \times 10^{-6}$ m^2/s. For our long period swells, twice the amplitude attenuation of equation (A10) in *Liu and Mollo-Christensen* [1988] gives a spatial attenuation for the energy at a rate $\alpha_\nu \simeq k\sqrt{(\nu 2\pi f/2)/C_g}$, where C_g is the group speed. This gives $\alpha_\nu = 1.6\times10^{-7}$ m^{-1} for $T = 25$ s. We multiply these values by a tuning coefficient C_ν. Scattering is represented by a constant spatial decay rate for the energy α_s, multiplied by a similar tuning coefficient, C_s, and combined with an isotropic redistribution of the scattered energy. Since this dissipation and scattering are linear functions of the directional spectrum, these are integrated exactly for a spatially uniform sea state, following *Ardhuin and Herbers* [2002].

We have tested a number of variations on these numerical choices, and they have a very limited numerical impact. The spatial resolution and integration time step used were verified to correspond to a well-converged numerical solution, because the evolutions due to scattering or dissipation used here are weak at the scale of the 12.5 km grid resolution. The impact of an isotropic scattering compared to a narrower forward or backscattering had limited impact on the solution once the model was adjusted to reproduce the observed wave height. Indeed a narrow forward scattering requires a stronger scattering coefficient to arrive at the same wave height. The influence of the ice on the group speed is expected to be limited to a 4% faster propagation for an ice thickness of 4 m and wave periods of 24 s.

The energy balance we use corresponds to a combination of the ice-covered Boltzman equation source terms as in *Meylan and Masson* [2006], with our two adjustable coefficients C_ν and C_s scaled by the ice concentration c, and the open water source terms S_o scaled by $1-c$,

$$\frac{\partial F(f,\theta)}{\partial t} + \mathbf{C}_g \cdot \boldsymbol{\nabla} E = (1-c)S_o + cC_g \times \left\{ C_s \alpha_s \int_0^{2\pi} \left[F(f,\theta') - F(f,\theta)\right] \mathrm{d}\theta' - C_\nu \alpha_\nu E \right\}. \tag{7}$$

Here $\mathbf{C}_g$ is the group velocity vector with a norm C_g. This scaling by the concentration means that the ice source terms jump from zero in ice-free grid points to their full value in the ice, as the concentration is very

near 90% for most of the propagation path in the ice. Such a uniform dissipation and scattering is a strong simplification of the real-world conditions, where we expect to have much stronger scattering in the MIZ compared to within the pack. Nonetheless, this formulation is useful for illustrating the different effects that scattering and dissipation have upon the wave field. We note that the redistribution of the scattered energy in all directions makes the effective attenuation rate due to scattering $\alpha = (\partial E/\partial t)/E$ much smaller than α_s.

Two simulations will be discussed, one dominated by scattering and the other by dissipation. The scattering and dissipation strengths were adjusted to reproduce the maximum value of 2.5 cm wave height recorded in the ice on 12 February; this is why we define $\alpha_s = 8 \times 10^{-6}$ m^{-1}. Without dissipation ($C_v = 0$) energy would grow to very large values; thus, the molecular viscous dissipation has been retained in the scattering-dominated simulation, which is defined by $C_v = 1$ and $C_s = 1$. In the absence of scattering, viscous dissipation had to be increased by a factor of 12 and the dissipation-only simulation is defined by $C_v = 12$ and $C_s = 0$. It corresponds to a spatial attenuation rate for the energy $\alpha = 1.9 \times 10^{-6}$ m^{-1} for a period $T = 25$ s, decreasing like $T^{-3.5}$.

Figure 2 shows the modeled maps of swell heights and mean directions for the dissipation and scattering simulations at 18 UTC on 12 February, at a time when the measured waves have a peak period of 25 s at the tiltmeter.

In Figure 2a, the significant swell height is predicted by the dissipation-only scheme, using periods 19 to 28 s, and in Figure 2c with a narrower range of periods, 24 to 28 s. That latter figure shows a maximum swell height around 86°N 90°E and 78°N 80°E, associated with the 9 September storm, and the swell maximum that has not yet entered the ice, centered south of Svalbard, is from the September 10 storm. The reduced swell heights of the 9 September storm, not more than 3 cm near *Tara*, are due to the dispersion of the swell field and interaction with the sea ice. When a wider frequency range is used (Figure 2a), frequency dispersion leads to a broader distribution in the propagation direction.

Figures 2b and 2d show the significant swell height at the same time as Figure 2a but modeled using the scattering attenuation mechanism. In Figure 2d, the 9 February swell peaks can be seen at approximately 83°N 10°E, and 78°N 70°E. The incident open water swell propagation was, by definition, the same in both cases. Higher open water wave heights in Figures 2b and 2d, compared to Figures 2a and 2c, are due to waves backscattered from the ice in the open ocean.

The most striking result in Figure 2 is that, at the plotted time, the peak of the swell field modeled using the dissipative mechanism had propagated much farther into the ice than had the scattering-based peak. This is due to the increased path length that wave energy must follow in the scattering case, with energy being redirected by multiple scatterers within the pack ice. Thus, the resulting diffusion of wave energy in space is associated with a diffusion in time as well. This trapping of waves in the ice is akin to Anderson localization [*Anderson*, 1958], which was observed for water waves over random bottom topography by *Belzons et al.* [1988]. Furthermore, whereas energy reaches *Tara* via a single narrow beam in the dissipation run, it arrives from all the ice edges in the scattering run, with very different mean paths and arrival directions.

Figure 3 shows time series of significant wave height and directional spreading at the *Tara* experimental site, for both measured data and modeled results. The sea ice thickness, between 2 and 4 m according to submarine-based measurements reported by *Wadhams et al.* [2011], is expected to change the propagation time by up to 23% for a 20 s period but only 4% for 24 s, which is 1 h for a path of 1500 km. This speedup induced by the ice is only one third of the difference between the measured and modeled peak arrival, which is probably mostly due to model errors in the open ocean between Ireland and Svalbard.

More striking is the difference in duration of the swell event at the measurement location. The scattering run shows the wave energy peak arrival on 14 February, 2 days after the measurements, and the energetic event lasts for 7 days instead of the 2 well-separated events that are seen in the observations and dissipative model. This difference between scattering and dissipation is due to the longer propagation path caused by scattering as the waves bounce many times around the ice pack before being dissipated or propagating away. It is worth noting that, in the dissipative case, the third-order advection scheme used in the wave model [*Tolman*, 2002] is a key element for reproducing the sharp arrival time of such remote swells [*Wingeart et al.*, 2001].

As expected, the directional spread with the scattering mechanism is much wider than that with the dissipative mechanism (Figure 3b). At the swell energy peaks, the observed spreading was narrow, comparable

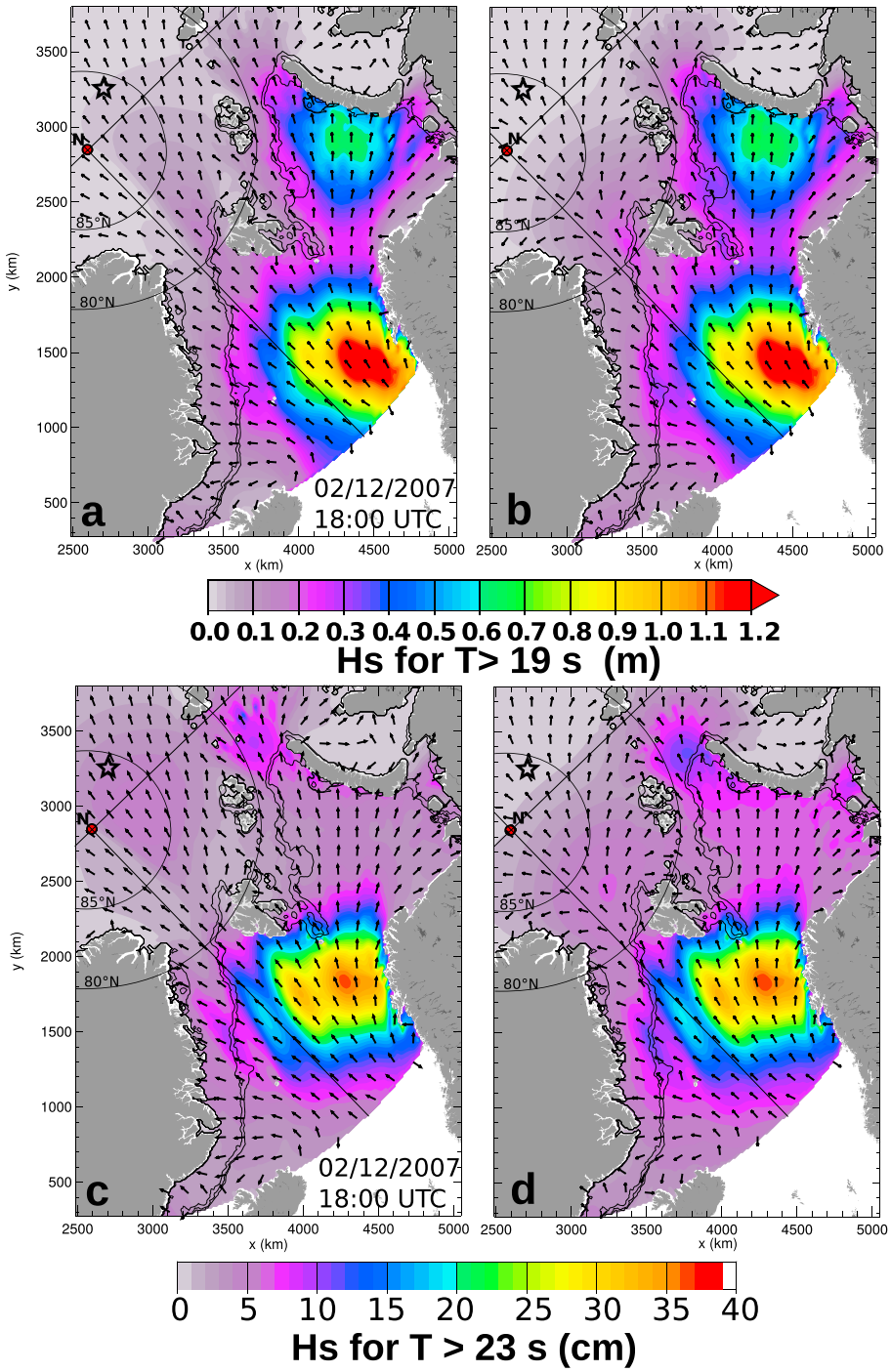

Figure 2. Modeled significant swell heights for periods (a, b) larger than 19 s and (c, d) larger than 25 s, using dissipation (Figures 2a and 2c) and scattering (Figures 2b and 2d). The solid lines mark the 15, 30, and 80% concentration in sea ice. The star, located at 85.6°N and 126.6°E marks the position of the tiltmeter near the *Tara* schooner on 13 February.

to the dissipative model case, and inconsistent with the scattering model. At times outside swell events, the observed spectra broadened significantly, while the dissipative model continued to show narrow spreading. These correspond to extremely small motions, that are likely due to ice movements forced by processes other than exterior wave motions, possibly the local wind [*DiMarco et al.*, 1991]. Only during strong wave events is the wave signal stronger than this background geophysical noise.

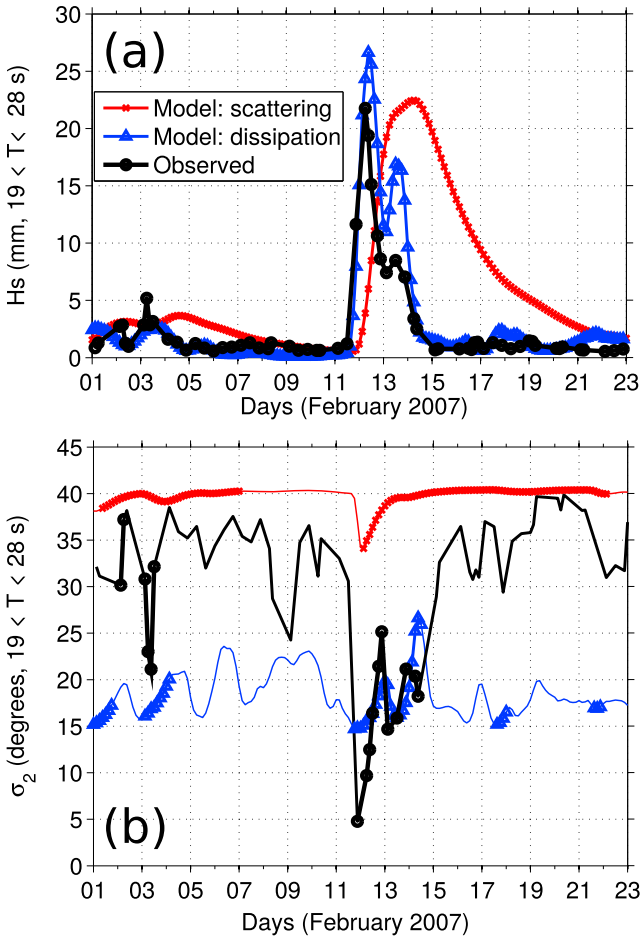

Figure 3. Time series of (a) significant wave height and (b) directional spreading measured and modeled at the tiltmeter. Values are calculated over the frequency band 0.037 to 0.04 Hz. In both panels, black lines are the observations, blue diamonds are from the dissipation-based model, and red triangles are from the scattering-based model. In Figure 3b we have highlighted in bold and with symbols the times when the corresponding wave height exceeds 2 mm.

4. Discussion and Conclusion

Waves recorded in the pack ice by *Wadhams and Doble* [2009] show well-separated swell arrivals with narrow directional spreading. In this work, we have modeled ocean surface gravity waves across the Arctic ice. This allowed us to investigate the relative importance of scattering and dissipation for swell attenuation in sea ice.

The model results clearly show that both the timing of the energy arrival and the directional properties of waves with periods 19 to 30 s recorded in the pack ice are inconsistent with an attenuation dominated by uniform scattering. This finding is consistent with the general result that scattering is mostly relevant for short wavelength, in particular, wavelengths comparable with the scales at which the ice thickness varies [e.g., *Squire et al.*, 1995]. Calculations not shown here with scattering confined to the marginal ice zone (defined here as the region with concentration between 0.2 and 0.8) can produce narrower directional spectra, but not as narrow as with dissipation alone, and they still have a delay of at least 6 h in the timing of the energy peaks and a long duration. The Wide-Swath SAR images available from Envisat for that event (just west of Svalbard, on 12 February at 11:23 UTC) show some barely visible modulation at the ice edge from which it is not possible to extract a wave spectrum. However, the part of that image in the water has a visible 600 m wavelength modulation, corresponding to 20 s waves, which look long crested, similar to such long swells in the water or the ice in recent Sentinel 1 data (see, e.g., http://bit.ly/1SXO91u or http://bit.ly/1SXNn4F).

We thus conclude that dissipation is the main source of attenuation of these long period swells. We note that, using an ice thickness transect from a different region of the Arctic where ice is likely thicker, *Squire et al.* [2009] predicted for $T = 25$ s, an attenuation of the wave energy due to scattering at a rate $\alpha = 2.6 \times 10^{-6}$ m^{-1}.

This is close to the dissipative attenuation required in our model, with a value $\alpha = 1.9 \times 10^{-6}$ m^{-1}. However, the directional spreading and time history of the wave energy are not compatible with such a uniform scattering in the entire pack ice. Differences in ice thickness and two- versus one-dimensional treatment of the ice scattering could be the reasons why the *Squire et al.* [2009] model does not apply to the case investigated here. The 2007 ice conditions between the ice edge and the measurement location are not well known, but there is a nearby submarine transect described in *Wadhams et al.* [2011] that reveals a large number of 10 m thick ridges, more than one per kilometer, in spite of a most frequent thickness around 2 m, and a mean thickness near 4 m at the ice edge.

For periods 20 to 25 s, the constant dissipation rate needed to obtain a reasonable agreement corresponds to a spatial decay of the energy ranging from $\alpha \simeq 4 \times 10^{-6}$ m^{-1} at $T = 20$ s, to $\alpha \simeq 2 \times 10^{-6}$ m^{-1} at $T = 25$ s. These are 12 times the effect of viscous friction below a smooth ice plate. This elevated dissipation is expected to be partly due to floe morphology, with ice floes known to have complicated keel structures, often exceeding 10 m below the mean ice level [*Doble et al.*, 2011]. Energy loss to turbulent kinetic energy dissipation is also expected to be important, particularly in the energetic MIZ. There is unfortunately little data available to parameterize that effect, except for some possibly related laboratory experiments [e.g., *Toffoli et al.*, 2015].

Finally, creep is another possible dissipative mechanism. The parameterization proposed in *Wadhams* [1973] gives a dissipation rate that scales like the wave height squared and the ice thickness to the fifth power. We use a value of the Glen flow law parameter consistent with the laboratory experiments of *Cole et al.* [1998] for cyclic loading, i.e., their creep constant $A = 10^{11}$ and a uniform ice temperature of 270 K gives a value of 10^7 s$^{1/3}$ for Wadham's parameter B. Creep produces a nonlinear dissipation that yields a fast decrease in wave height near the ice edge, turning into a much slower decay at larger distances, e.g., between 1000 and 1500 km for a wave period $T = 25$ s. At the location of Tara, this creep-induced dissipation added to the viscous dissipation with $C_v = 2$ yields a maximum wave height of 2.2 cm for an ice thickness of 4 m. This thickness is consistent with the submarine-based measurements of [*Wadhams et al.*, 2011], making the creep-induced dissipation a possible explanation for the observed decay.

Future field studies and detailed modeling efforts would do well to attempt to resolve these mechanisms, in order to allow a generalization of the dissipation rate observed here to other wave periods and regions. If creep effects associated with ice flexing are indeed the main mechanism for wave attenuation, the expected very strong dependence of the attenuation on the ice thickness may lead to a more widespread penetration of waves in the Arctic ice as it rapidly thins [*Lindsay and Schweiger*, 2015], with yet to be determined feedbacks on the ice and waves.

Acknowledgments

F. A. and P. S. are supported by Labex Mer via grant ANR-10-LABX-19-01, EU-FP7 project SWARP under grant agreement 607476 and ONR grant number N0001416WX01117. The *Tara* data were acquired under the DAMOCLES project, grant 018509 of the European Union 6th Framework Program. We gratefully acknowledge the assistance of the crew of *Tara*—particularly Hervé le Goff, Jean Festy, and Matthieu Weber—for maintaining the instrumentation during the drift. Field data are available from http://www.polarscientific.com/. Numerical model results are available at ftp://ftp.ifremer.fr/ww3/PAPERS/2016_GRL_Tara_ice_swell. In depth comments and suggestions by two anonymous reviewers helped clarify our analysis.

References

Anderson, P. W. (1958), Absence of diffusion in certain random lattices, *Phys. Rev.*, *109*, 1492–1505.

Ardhuin, F., and T. H. C. Herbers (2002), Bragg scattering of random surface gravity waves by irregular sea bed topography, *J. Fluid Mech.*, *451*, 1–33.

Ardhuin, F., T. H. C. Herbers, P. F. Jessen, and W. C. O'Reilly (2003), Swell transformation across the continental shelf. Part II: Validation of a spectral energy balance equation, *J. Phys. Oceanogr.*, *33*, 1940–1953.

Ardhuin, F., A. Rawat, and J. Aucan (2014), A numerical model for free infragravity waves: Definition and validation at regional and global scales, *Ocean Modell.*, *77*, 20–32.

Asplin, M. G., R. Galley, D. G. Barber, and S. Prinsenberg (2012), Fracture of summer perennial sea ice by ocean swell as a result of Arctic storms, *J. Geophys. Res.*, *117*, C06025, doi:10.1029/2011JC007221.

Belzons, M., E. Guazzelli, and O. Parodi (1988), Gravity waves on a rough bottom: Experimental evidence of one-dimensional localization, *J. Fluid Mech.*, *186*, 539–558.

Bennetts, L. G., and V. A. Squire (2012), On the calculation of an attenuation coefficient for transects of ice-covered ocean, *Proc. R. Soc. London, Ser. A*, *468*, 132–162, doi:10.1098/rspa.2011.0155.

Cole, D. M., R. A. Johnson, and G. D. Durell (1998), Cyclic loading and creep response of aligned first-year sea ice, *J. Geophys. Res.*, *103*(C10), 21,751–21,758.

Collins, C. O., R. III W. E., A. Marchenko, and A. V. Babanin (2015), In situ measurements of an energetic wave event in the Arctic marginal ice zone, *Geophys. Res. Lett.*, *42*, 1863–1870, doi:10.1002/2015GL063063.

Delpey, M., F. Ardhuin, F. Collard, and B. Chapron (2010), Space-time structure of long swell systems, *J. Geophys. Res.*, *115*, C12037, doi:10.1029/2009JC005885.

DiMarco, R. L., J. P. Dugan, and W. W. Martin (1991), Ice motions forced by boundary layer turbulence, *J. Geophys. Res.*, *96*(C6), 10,617–10,624.

Doble, M. J., H. Skourup, P. Wadhams, and C. A. Geiger (2011), The relation between Arctic sea ice surface elevation and draft: A case study using coincident AUV sonar and airborne scanning laser, *J. Geophys. Res.*, *116*, C00E03, doi:10.1029/2011JC007076.

Doble, M. J., and J.-R. Bidlot (2013), Wave buoy measurements at the Antarctic sea ice edge compared with an enhanced ECMWF WAM: Progress towards global waves-in-ice modelling, *Ocean Modell.*, *70*, 166–173, doi:10.1016/j.ocemod.2013.05.012.

Dumont, D., A. Kohout, and L. Bertino (2013), A wave-based model for the marginal ice zone including a floe breaking parameterization, *J. Geophys. Res.*, *116*, C00E03, doi:10.1029/2010JC006682.

Ezraty, R., F. Girard-Ardhuin, and Piollé J. F. (2007), Sea-ice drift in the central Arctic combining QuikSCAT and SSM/I sea ice drift data. User's manual, version 2.0, *Tech. Rep.*, Ifremer.

Hanafin, J., et al. (2012), Phenomenal sea states and swell radiation: A comprehensive analysis of the 12–16 February 2011 North Atlantic storms, *Bull. Am. Meterol. Soc.*, *93*, 1825–1832.

Kuik, A. J., G. P. van Vledder, and L. H. Holthuijsen (1988), A method for the routine analysis of pitch-and-roll buoy wave data, *J. Phys. Oceanogr.*, *18*, 1020–1034.

Lindsay, R., and A. Schweiger (2015), Arctic sea ice thickness loss determined using subsurface, aircraft, and satellite observations, *The Cryosphere*, *9*, 269–283, doi:10.5194/tc-9-269-2015.

Lique, C., J. D. Guthrie, M. Steele, A. Proshutinsky, J. H. Morison, and R. Krishfield (2014), Diffusive vertical heat flux in the Canada Basin of the Arctic Ocean inferred from moored instruments, *J. Geophys. Res. Oceans*, *119*, 496–508, doi:10.1002/2013JC009346.

Liu, A. K., and E. Mollo-Christensen (1988), Wave propagation in a solid ice pack, *J. Phys. Oceanogr.*, *18*, 1702–1712.

Maslanik, A., C. Fowler, J. Stroeve, S. Drobot, J. Zwally, D. Yi, and W. Emery (2007), A younger, thinner Arctic ice cover: Increased potential for rapid, extensive sea-ice loss, *Geophys. Res. Lett.*, *34*, L24501, doi:10.1029/2007GL032043.

Meylan, M., V. Squire, and C. Fox (1997), Towards realism in modeling ocean wave behavior in marginal ice zones, *J. Geophys. Res.*, *102*(C10), 22,981–22,991, doi:10.1029/97JC01453.

Meylan, M. H., and D. Masson (2006), A linear Boltzmann equation to model wave scattering in the marginal ice zone, *Ocean Modell.*, *11*, 417–427.

Montiel, F., V. A. Squire, and L. G. Bennetts (2016), Attenuation and directional spreading of ocean wave spectra in the marginal ice zone, *J. Fluid Mech.*, *790*, 492–522, doi:10.1017/jfm.2016.2.

Mosig, J. E. M., F. Montiel, and V. A. Squire (2015), Comparison of viscoelastic-type models for ocean wave attenuation in ice-covered seas, *J. Geophys. Res. Oceans*, *120*, 6072–6090, doi:10.1002/2015JC010881.

Munk, W. H., G. R. Miller, F. E. Snodgrass, and N. F. Barber (1963), Directional recording of swell from distant storms, *Philos. Trans. R. Soc. London, Ser. A*, *255*, 505–584.

Perovich, D., B. Light, H. Eicken, K. Jones, K. Runciman, and S. Nghiem (2007), Increasing solar heating of the Arctic Ocean and adjacent seas, 1979âĂŞ2005: Attribution and role in the ice-albedo feedback, *Geophys. Res. Lett.*, *34*, L19505, doi:10.1029/2007GL031480.

Queffeulou, P., and D. Croizé-Fillon (2010), Global altimeter SWH data set, version 7, May 2010, *Tech. Rep.*, Ifremer. [Available at http://tinyurl.com/2cj5sez.]

Rascle, N., and F. Ardhuin (2013), A global wave parameter database for geophysical applications. Part 2: Model validation with improved source term parameterization, *Ocean Modell.*, *70*, 174–188, doi:10.1016/j.ocemod.2012.12.001.

Renner, A. H. H., S. Gerland, C. Haas, G. Spreen, J. F. Beckers, E. Hansen, M. Nicolaus, and H. Goodwin (2014), Evidence of Arctic sea ice thinning from direct observations, *Geophys. Res. Lett.*, *41*, 5029–5036, doi:10.1002/2014GL059983.

Saha, S., et al. (2010), The NCEP Climate Forecast System Reanalysis, *Bull. Amer. Meterol. Soc.*, *91*, 1015–1057.

Squire, V., J. Dugan, P. Wadhams, P. Rottier, and A. Liu (1995), Of ocean waves and sea ice, *Annu. Rev. Fluid Mech.*, *27*(3), 115–168.

Squire, V. A., and S. C. Moore (1980), Direct measurement of the attenuation of ocean waves by pack ice, *Nature*, *283*, 365–368.

Squire, V. A., G. L. Vaughan, and L. G. Bennetts (2009), Ocean surface wave evolvement in the Arctic Basin, *Geophys. Res. Lett.*, *36*, L22502, doi:10.1029/2009GL040676.

Stroeve, J., L. C. Hamilton, C. M. Bitz, and E. Blanchard-Wrigglesworth (2014), Predicting September sea ice: Ensemble skill of the SEARCH Sea Ice Outlook 2008–2013, *Geophys. Res. Lett.*, *41*, 2411–2418, doi:10.1002/2014GL059388.

Thomson, J., and W. E. Rogers (2014), Swell and sea in the emerging Arctic Ocean, *Geophys. Res. Lett.*, *41*, 3136–3140, doi:10.1002/2014GL059983.

Toffoli, A., L. G. Bennetts, M. H. Meylan, C. Cavaliere, A. Alberello, J. Elsnab, and J. P. Monty (2015), Sea ice floes dissipate the energy of steep ocean waves, *Geophys. Res. Lett.*, *42*, 8547–8554, doi:10.1002/2015GL065937.

Tolman, H. L. (2002), Alleviating the garden sprinkler effect in wind wave models, *Ocean Modell.*, *4*, 269–289.

Wadhams, P. (1973), Attenuation of swell by sea ice, *J. Geophys. Res.*, *78*(18), 3552–3563.

Wadhams, P. (1975), Airborne laser profiling of swell in an open ice field, *J. Geophys. Res.*, *80*, 4520–4528, doi:10.1029/JC080i033p04520.

Wadhams, P. (1978), Wave decay in the marginal ice zone measured from a submarine, *Deep Sea Res.*, *80*(33), 4520–4528.

Wadhams, P., and M. J. Doble (2009), Sea ice thickness measurement using episodic infragravity waves from distant storms, *Cold Reg. Sci. Technol.*, *56*, 98–101, doi:10.1016/j.coldregions.2008.12.002.

Wadhams, P., V. A. Squire, D. J. Goodman, A. M. Cowan, and S. C. Moore (1988), The attenuation rates of ocean waves in the marginal ice zone, *J. Geophys. Res.*, *93*(C6), 6799–6818, doi:10.1029/JC093iC06p06799.

Wadhams, P., N. Hughes, and J. Rodrigues (2011), Arctic sea ice thickness characteristics in winter 2004 and 2007 from submarine sonar transects, *J. Geophys. Res.*, *116*, COOE02, doi:10.1029/2011JC006982.

Welch, P. D. (1967), The use of fast Fourier transform for the estimation of power spectra: A method based on time averaging over short, modified periodograms, *IEEE Trans. Audio and Electroacoustics*, *15*(2), 70–73.

Williams, T. D., L. G. Bennetts, V. A. Squire, D. Dumont, and L. Bertino (2013a), Wave-ice interactions in the marginal ice zone. part 1: Theoretical foundations, *Ocean Modell.*, *70*, 81–91, doi:10.1016/j.ocemod.2013.05.010.

Williams, T. D., L. G. Bennetts, V. A. Squire, D. Dumont, and L. Bertino (2013b), Wave-ice interactions in the marginal ice zone. Part 2: Numerical implementation and sensitivity studies along 1D transects of the ocean surface, *Ocean Modell.*, *71*, 92–101, doi:10.1016/j.ocemod.2013.05.011.

Wingeart, K. M., T. H. C. Herbers, W. C. O'Reilly, P. A. Wittmann, R. E. Jensen, and H. L. Tolman (2001), Validation of operational global wave prediction models with spectral buoy data, in *Proceedings of the 4th International Symposium Ocean Wave Measurement and Analysis*, pp. 590–599, ASCE, San Francisco, Calif., doi:10.1061/40604(273)61.